Photoluminescence: science and applications

Jacques Lefebvre,[1] Shigeo Maruyama[2] and Paul Finnie[1]

[1]*Institute for Microstructural Sciences, National Research Council of Canada, Montreal Road, Ottawa, Ontario K1A 0R6, Canada*

[2]*The* Department of Mechanical Engineering, The University of Tokyo, 7-3-1 Hongo, Bunkyo-ku, Tokyo 113-8656, Japan

Abstract. In the past five years photoluminescence (PL) of SWNTs has gone from discovery to one of the most actively researched areas, with broad impact on the basic science of SWNTs, as well as the promise of applications. The simplest free-carrier models of perfect semiconducting SWNTs in vacuum predict that they have direct bandgaps and therefore should be efficient light absorbers and emitters. Experimentally, isolating SWNTs from environmental interactions proves crucial to observing this strong PL. The Coulomb interaction enhanced by one-dimensional confinement requires that excitonic models be invoked to understand PL features. Prepared properly, SWNTs are strong PL emitters, with good quantum yield, showing principal PL peaks with characteristic lineshapes and (*n*,*m*) dependent emission and absorption energies, as well as a rich absorption spectrum. PL has emerged as an important characterization tool for determining (*n*,*m*) and (*n*,*m*) distributions, albeit with some limitations. Extrinsic factors, such as chemical environment, temperature, electric and magnetic field, or intrinsic factors, such as phonons, are manifest in SWNT PL. Possible applications in sensing, biological markers, and optoelectronics are beginning to emerge from current research in SWNT PL.

1. Introduction

The first report of photoluminescence (PL) in single walled carbon nanotubes (SWNTs) dates to 2002[1], and in the intervening half-decade there has been tremendous progress including a great number of fundamental studies of SWNT PL, the emergence of PL methods as basic characterization tools, and the early exploration of PL related applications. The term "photoluminescence" describes any process in which light is absorbed by a medium, generating an excited state, and then light of lower frequency is re-emitted upon recombination to a ground state. In the currently accepted picture of SWNT PL, when a SWNT is photo-excited, electron-hole pairs are created in form of excitons, which are subsequently annihilated with the emission of photons. Of special interest for fundamental science is the strong, one dimensional confinement with its consequences for PL characteristics. The SWNT represents a unique model system for which the range of diameters and chiralities available through synthesis allows for a quasi-continuous tuning of exciton confinement energy and symmetry. The SWNT also constitutes a bridge between bulk crystals traditionally studied by physicists, and molecules traditionally studied by chemists, and as such its optical properties can be understood in terms of either as a starting point, and the methods of both disciplines can be applied.

The aim of this chapter is to outline the PL related properties of SWNTs and how they are presently understood. The number of publications is large and growing rapidly, and cannot be fully explained in such a short review. Nonetheless, we hope the chapter will provide a good starting point for those interested in SWNT PL. Some important topics are treated very briefly because they are covered in detail in other chapters of this book. The chapter consists of the following sections: Section 2, *"Basic Photoluminescence Spectroscopy of Isolated Nanotubes"*, gives the basic description of optical processes in SWNTs, including absorption, luminescence, photoluminescence excitation, effects of sample preparation, and excitonic effects . Section 3, *"Spectroscopic Properties of Nanotube Photoluminescence"* presents the spectral characteristics of SWNT PL including linewidths, lineshapes, quantum efficiency, and phonon-related features. Section 4, *"Physical and chemical effects"*, gives an overview of the effects on the PL of various physical parameters such as temperature, strain, electric and magnetic fields, and chemical doping. Finally, section 5 *"Applications"* looks beyond the fundamental science to explore some of the possible PL-related applications of SWNTs which are currently under exploration. Finally, section 6 provides a summary and outlook for the field of SWNT PL-related research in the next few years.

2. Basic Photoluminescence Spectroscopy of Isolated Nanotubes

2.1 Model. In SWNTs, the band structure is a series of one-dimensional subbands arising from the periodic boundary conditions imposed by wrapping the graphene sheet. The dominant "allowed" optical electronic transitions connect bands with the same index. These longitudinal transitions are labeled E_{11} and E_{22} (more generally E_{ii}, i=1,2,3…) in Fig. 1, and are allowed for light polarized along the nanotube axis. In the simplest physical picture of PL, light absorption occurs at E_{ii}, and after some relaxation process, recombination occurs at E_{11}. A schematic of the band structure of an SWNT and the PL process at this level of approximation is shown in Fig. 1a. Absorption and emission energies are intimately connected to the nanotube diameter and chirality. The longitudinal transitions can be described to leading order by:

$$E_{11} = 2\gamma_o a d^{-1} + (-1)^{\nu} \frac{t_{11}\cos(3\theta)}{d^2}, \quad (1)$$

$$E_{22} = 4\gamma_o^* a d^{-1} - (-1)^{\nu} \frac{t_{22}\cos(3\theta)}{d^2}, \quad (2)$$

where $\gamma_o^{(*)}$ (2.6-3.0 eV), t_{11} and t_{22} are free parameters related the onsite energy and to the hopping integrals, respectively, and a is the lattice parameter (2.42 Å), d is the nanotube diameter, and θ is the nanotube chiral angle. For polarization perpendicular to the tube axis, transitions are allowed between states belonging to bands which differ by one in band index. For example, an electron is promoted from the highest valence band (v_1 in Fig.1a) to the second lowest conduction band (c_2), an E_{12} transition. The large geometrical anisotropy of carbon nanotubes, and consequently its dielectric environment, leads to a strong suppression of transverse transitions (the "antenna effect", see Chapter 7).[2] Within a non-interacting picture, the

tranverse E_{12} (and E_{21}) transitions appear halfway in energy between E_{11} and E_{22}. Experimentally, the longitudinal and transverse configurations are most commonly probed. However, light propagation along the tube axis will also give rise to interesting optical transitions. For example, chiral tubes will show different responses to left and right circular polarization for light propagation along the tube axis ("dichroic effects"). Such transitions should also be weak due to the antenna effect.

Although non-interacting pictures are useful models, the effect of the Coulomb interaction must be taken into account to properly describe SWNT PL. In one dimension, charged particles are compelled to interact more strongly, and the peaked DOS, the reduced charge screening, and the reduced phase space are all factors enhancing the effect of Coulomb interaction. This was already recognized in the earliest PL work on SWNTs,[2] and it is PL experiments that have since provided the most direct evidence of these Coulomb effects. Chapters 6 and 7 provide full treatments of exciton theory. In particular Fig. XX of Chapter 6 shows how the absorption spectrum evolves as the strength of Coulomb interaction is increased.[3]

A basic description of interaction effects on peak positions is needed to understand PL data. First, positions of the free-particle E_{ii} transitions are pushed apart by a self-energy renormalization term. At the same time, an electron and a hole will bind together via their mutual Coulomb interaction, and these bound excitonic states lie well below (~0.3 eV) the free particle states, more or less counteracting the repulsive self-energy correction. Each optical transition (e.g. E_{11} or E_{22}) and its related bands in the single particle picture generates a set of exciton bands with its own selection rules. The unbound (or "continuum") states still exist, but the oscillator strength shifts from the free electron-hole pair to the optically allowed ground state exciton. When using the notation E_{ij} in PL experiment now, one generally refers to the bound optically active excitonic bands.

Within the excitonic picture, experiment indicates that equation 1 and 2 remain a reasonable approximation, but with a different set of parameters for γ_0, γ_0^*, t_{11} and t_{22}. This can be understood in part because the exciton dispersion, though different from the single particle dispersion, still must incorporate the same graphene-related symmetries. Thus, measurement of PL transition energies can provide evidence for excitons in SWNTs.

2.2 Absorption. Absorption is the fundamental first step to any PL emission. Historically, optical absorption on SWNTs preceded PL measurements by several years,[4,5] principally because, regardless of preparation, nanotubes can absorb light, while nanotubes must be specially prepared to be good PL emitters. These samples consisted of large ensembles of SWNTs, which would typically be bundled into ropes and contain some level of impurities, for example catalyst residues and non-nanotube carbonaceous material. A typical absorption spectrum from SWNTs as compared to graphite is shown in Fig. 2a.[6] Above 2.0 eV, the spectrum is relatively featureless and generally similar to graphite. At lower energies however, both spectra differ significantly, with the SWNT sample showing three broad peaks labeled A, B and C (~0.1 to ~0.4 eV FWHM). The origin of these peaks was associated with the lowest allowed transition in semiconducting SWNTs (peak A, typically referred to as E_{11}), the second allowed transition of the same semiconducting SWNTs (peak B, or E_{22}), and the first peak in the JDOS of the metallic nanotubes (metallic according to mod(n-m,3)=0). The corresponding transitions are labeled in Fig. 1b.

Despite the fact that SWNTs have sharply peaked density of states, the peaks found in the absorption spectra are broad. Beyond lifetime broadening, several factors affect the absorption linewidth for materials in general. Specifically for SWNTs, sample heterogeneity is the dominant factor. An ensemble of nanotubes most often consists of many different species (n,m), each with a different set of absorption peaks, adding up to produce the broad peak reflecting to first order a diameter distribution. In addition, even if the sample consisted of only a single nanotube species, interaction with the environment, either through bundling or contact with other material, can broaden spectral features. Fig. 2c illustrates how bundling severely broadens the series of narrow absorption peaks (~25 meV) obtained on ensembles of individual SWNTs.

2.3 Photoluminescence from isolated SWNTs. The breakthrough which began the era of PL studies on SWNTs was at first one of purification, where isolated SWNTs could be separated from bundled ones.[1] The absorption spectra of the separated SWNTs showed series of sharp peaks (~25 meV), rather than the broad peaks seen for bundles. (See Fig. 3a and Fig. 2c). In stark contrast to bundle samples, these separated SWNTs in suspension also showed sharp fluorescent peaks in the near infrared when excited with laser illumination in the visible. Fig. 3a shows the emission spectrum, which has virtually identical energies and similar linewidths (~25 meV) as the absorption spectrum. This led to the conclusion that the same

states are responsible for both processes and that the luminescence involves transitions between band extrema in semiconductors (i.e. from E_{11}). Since this original work, many other recipes using a variety of surfactants have been tested by several groups. This is presently the dominant method to obtain PL spectra from SWNTs.

For basic studies and for many applications, it is useful to immobilize the nanotubes. The addition of PVP to the suspensions produced a solid with similar luminescence efficiencies to the aqueous suspension. There are also alternative methods of isolating individual SWNTs that predate these methods. One approach to isolating SWNTs from their surroundings and preventing bundling is to synthesize them on textured substrates, for instance on a substrate patterned with pillars or trenches.[7] Chemical vapor deposition was found to be an effective method to produce such samples, where large numbers of isolated single SWNTs bridging pillar to pillar can be synthesized.[7,8] Such nanotubes are surrounded only by gas ambient – there is no surfactant or solvent to interact with the nanotube surface. In a first experiment with such samples, laser illumination showed no NIR photoluminescence from the flat surfaces known to have abundant SWNTs.[9] But on pillars bridged by sparse networks of SWNTs, sharp peaks were observed (Fig. 3b). Notably these peaks are substantially sharper (~10 meV) than the micelle wrapped SWNTs. Wavelength dependent excitation confirmed that these peaks are the same E_{11} transitions observed for micelle wrapped SWNTs. Such SWNTs have spectral properties in many ways superior to the micelle wrapped nanotubes (see Section 3.1 for details), and single nanotube studies[10] are no more difficult than ensemble studies. These freely suspended SWNTs, either in air or some other gas ambient, are ideal for spectroscopic studies, and they prove to be essential for the fundamental understanding of luminescent processes in SWNTs.

2.3 Photoluminescence excitation map. SWNTs have a unique, species-dependent optical absorption spectrum. An alternative probe of the energy band structure that is closely related to optical absorption is photoluminescence excitation (PLE) spectroscopy. In PLE the PL intensity is recorded while the excitation wavelength is changed. A maximum in intensity is found whenever the excitation energy passes through an absorption resonance from which relaxation to a PL emitting transition occurs. One can build up a three-dimensional "map" showing luminescent intensity vs. emission and excitation wavelength. An example of a PLE map is shown in Fig. 4a.[11] The intensity of luminescence is plotted on a color scale, with the emission wavelength along the x-axis and the excitation wavelength along the y-axis. This particular PLE map is for rather large diameter nanotubes, and the excitation energy extends over a relatively large range.

A PLE map obtained from an ensemble of SWNTs produces an intriguing pattern of spots such as in Fig. 4a, each representing a single (n,m) species. The so-called "fingerprint region" is visible in the center of the plot. Each spot in this region comes from resonant absorption into E_{22} with emission at E_{11}, for a given (n,m) species of nanotube.[12,13] The link between the (E_{11}, E_{22}) spots on the photoluminescence excitation map and their connection to specific (n,m) represents a fundamental result in nanotube photophysics and is discussed in detail in Chapter 3. PLE mapping has already emerged as an important method of identifying the (n,m) species in a given sample. This *(n,m)* assignment provides an alternative way to construct a "Kataura plot" (Fig. 4b),[4] which is complementary to Raman-derived plots. In such a plot, E_{11} and E_{22} resonances are plotted versus the nanotube diameter.

That the PLE map shows (n,m) dependent spots can be understood from the dispersion of graphene and the cutting lines associated with each (n,m) species. Conceptually, for a linear dispersion with no chiral angle dependence, an excitation map would show up as a series of spots distributed along a straight line with slope 2. Deviations from nonlinearity would not change the map qualitatively, but would only put E_{22} at some constant factor away from E_{11}. The SWNT however, possesses a trigonal symmetry of bonding similar to graphene, and therefore, the dispersion relation contains a term to reflect this distortion away from a circle. A PLE map including trigonal warping effects would fan out compared with the linear case, with two sets of branches on either side of the slope 2 median. Small *n-m* points (near armchair) sit close to the median line, and large *n-m* (towards zigzag) are farther away. The set of spots below the median (small E_{22} energy for a given E_{11}) belong to mod2 "family" (as defined by mod(n-m,3)=2), and the upper set to the mod1 family. This separation comes from the fact that mod1 and mod2 families sample opposite sides of energy contours. The effect of the trigonal warping term is amplified in PLE maps since the E_{11} and E_{22} cutting lines sample opposite sides of the energy dispersion. Experimentally, the median line is found to be around 1.7, and the deviation from 2 is attributed to self energy corrections to the energy dispersion.

The geometrical meaning of the *n-m* "family" is simple. Nanotubes with the same *n-m* value have fairly similar chiral angles but varying diameter. Another important grouping is the 2*n*+*m* "family", and this family can also be seen on the Kataura plot (Fig. 4b). Each set of peaks peeling away from the central line in the Kataura plot belongs to a single 2*n*+*m* family. The geometrical meaning of the 2*n*+*m* family is also simple and arises from the projection of the chiral vector onto the first primitive lattice vector, i.e. the projection of the chiral vector onto the zigzag line. SWNTs belonging to a given *2n*+*m* family are fairly similar in diameter, while the chiral angle varies.

Beyond (E_{11}, E_{22}) spots, a number of additional spectral features are evident in a PLE map. For example, the vertical streakiness in the map results from off-resonance absorption, which is typically a factor of ten or more weaker than on-resonance. Also, at the bottom right in Fig. 4a (λ<500 nm), a second "fingerprint" region appears as a kind of "echo" of the first fingerprint region. This corresponds to resonant excitation at E_{33} or E_{44} and emission at E_{11}. Like the first fingerprint, these resonances too, could be used for (*n*,*m*) assignment. Another kind of feature is the line labeled *G*, and also the much weaker line labelled *G*'. These show resonant absorption at levels which are a phonon frequency above $E_{11,}$ in this case the *G* (or *G*') phonon. Many such phonon echoes are now known, originating both from E_{11} and E_{22} and will be discussed in the next section. Importantly, pure Raman features some phonon energy below the excitation energy are often seen in PLE maps when laser excitation is used, particularly as combination modes (e.g. 2D+2G). [14] Finally, the bright line along the top, where the excitation wavelength and emission wavelength are almost equal, is mostly an experimental artifact caused by the lack of rejection of the excitation source. However, some real structure is visible here, originating from E_{11} absorption resonances, which are broader than the rejection of the optical setup.

While PLE maps are qualitatively similar for SWNT samples prepared with various methods, detailed analysis can reveal some significant differences. For example, Fig. 5 shows a map from SWNTs in free space with the SDS wrapped data of Ref. [12] plotted for comparison.[14] One immediately sees the same pattern of spots, and they can be related one-to-one to the surfactant based assignment. The micelle encapsulated emission peaks are slightly redshifted (28 meV on average for E_{11}). This shift is explained by dielectric screening produced by the solution surrounding the nanotubes.[3] The magnitude of the shift can be understood with reference to exciton models. However it is not trivial, since two effects opposite in sign shift the energy peak position, namely the self energy which increases the energy and the exciton binding energy which decreases it. The overall redshift of optical resonances was predicted theoretically. (See also section 4 and Chapter 8 of this volume.)

Depending on the details of the sample preparation, PLE maps can evolve from well-resolved peaks to broad unresolved features. In some cases, light emission observed from bundles was attributed to non-radiative relaxation and blackbody emission accompanying transient heating.[15] Recently, detailed analysis of PLE maps revealed that excitons can transfer to a neighboring nanotubes and emit light.[16] Structures closely related to individual, isolated SWNTs are also likely to emit PL in some cases. For example, preliminary PL experiments on double walled carbon nanotubes (DWNTs) have been performed, though with quite different results.[17,18]

2.4 Exciton Picture. In general, excitonic effects are important in low dimensional systems and similarly, excitons are expected to be important in SWNT PL: early experimental work alludes to their importance,[12] and at the time some excitonic effects were already predicted.[2] The excitonic picture is discussed in full detail in Chapter 6 and 7.

One early line of evidence for the need to use excitons to explain the PL data is the ratio problem. [19,20] The ratio of E_{22}/E_{11} for linear energy dispersion within the simplest tight binding model is 2. In more physical models of the single particle dispersion, "trigonal warping" other trigonally symmetric terms and diameter dependent curvature effects distort the shape of the dispersion and cause this ratio to deviate from 2. However, these distortions vanish in the limit of large SWNT radius (i.e near the *K*-point of the graphene dispersion). Thus the limit of E_{22}/E_{11} for large diameter SWNTs should go to 2. Extrapolating from the PLE mapping data, the ratio rather goes to ~1.7.[12,13]

The ratio problem can be understood if Coulomb interaction is included even in the simplest model with linear dispersion.[20] While the electronic (single particle) bandgaps scale roughly as 1/*d*, the Coulomb interaction has two contributions, excitonic and self-energy corrections. For large nanotube diameters, excitonic corrections vanish but self-energy corrections present in graphene remains. These are repulsive contributions which increase the values of both E_{11} and E_{22}, in such a manner that the average

ratio to become smaller than 2. The magnitude of the deviation is determined by the strength of the Coulomb interaction, and consequently is sensitive to the dielectric constant.

More evidence for excitons in SWNT is provided by a two-photon PLE experiment.[21,22] Conventional PL is a one-photon (linear) process and the absorption of a single photon causes the transition from the ground state to an excited state. The emission is also usually a single photon process. Recombination occurs across the bandgap with the emission of a single photon. However, at high excitation power densities, two photon absorption (TPA) can occur at an appreciable rate. TPA and one photon absorption (OPA) obey different selection rules. In conventional semiconductor materials, the difference between OPA and SPA has been used to demonstrate excitonic effects. Two groups have performed this type of experiment on SWNTs, showing that the TPA data is incompatible with the single particle picture of SWNT photoluminescence.

In one-dimension, excitonic states can be described by a hydrogen-like Rydberg series (*s*,*p*,*d*…) of bands below the single particle bandgap. For SWNTs, this represents an oversimplification; nonetheless this description provides some useful insights (For a more complete picture of excitonic states, see Chapter 6.). Excitonic states have definite parity with respect to a plane perpendicular to the tube axis. For transitions polarized along the tube axis, which are usually dominant in SWNT photoluminescence, OPA selection rules dictate that the initial and final states have opposite parity. In TPA such transitions have the same parity. In the Rydberg model, OPA absorption excites the lower lying *s*-like exciton, while TPA excites the *p*-like excited exciton state. This simple model was initially used to describe TPA but proper account of symmetries is required to reflect the chirality of SWNTs. Excitation with two photons will result in an absorption peak higher than the one photon peak. The process of two photon absorption followed by one photon photoluminescence emission in the excitonic picture is illustrated schematically in Fig. 1b.

In contrast, the single particle picture has only excitations into a continuum, and thus there is no selection rule to separate one and two photon processes. One and two photon absorption should both take place at the bandgap as measured by PL. A deviation of the two photon absorption peak from the photoluminescence emission peak (or one photon absorption peak) is a signature of excitonic effects. This is precisely what is observed in PL experiment as shown in Fig 6c. The absorption peak for the single particle picture would sit along a line at twice the emission wavelength. There is, however, an approximately 0.3 eV shift, representing the difference between the one and two photon states. The exciton binding energy can be estimated from this difference, but the exact number is model dependent. In any case, this represents a significant fraction the electronic bandgap, and is much larger than found in bulk semiconductors or two-dimensional confined semiconductor heterostructures.

3. Spectroscopic Properties of Nanotube Photoluminescence

3.1 Lineshape. As described in the previous section, the electronic DOS is strongly peaked at the band edge with the consequence of limited thermal broadening. Even if higher energy states can become thermally occupied at finite temperature, the lower density for those states reduces their relative contribution to the PL intensity. This reduced dimensionality should be reflected in PL linewidths. Indeed, air suspended SWNTs have emission linewidths at 300K as small as 9 meV, significantly smaller than the thermal energy of 25meV.[10] The early reports from surfactant SWNTs showed broader Lorentzian peaks of about 25 meV (FWHM).[1] For other preparation methods, broader linewidths of order of 50 meV have been reported.[23] The broader linewidth of these surfactant SWNTs as compared to air suspended SWNTs might by due to inhomogenous surfactant coatings, bundling effects, or due to damage or cutting due to the relatively aggressive suspension process. More recently narrow linewidths have been obtained from individual surfactant SWNTs

For air-suspended SWNTs the lineshape is systematically asymmetric, with a sharper rise on low-energy side and a more gradual fall-off at high energy (Fig 7).[10] Some surfactant SWNTs with narrow PL linewidth reproduce this shape.[24] Interestingly, this shape qualitatively reproduces a 1D DOS, but the connection of the lineshape to the DOS has not been separately confirmed. Individual nanotubes prepared by drying a drop of dispersion on glass have a single Lorentzian lineshape with approximately 25 meV linewidth.[25]

It seems likely that the narrow linewidths are intrinsic. Clearly, lifetime broadening can be excluded since PL radiative lifetime is estimated to be of order of nanoseconds, which implies μeV linewidths. Since excitons in SWNTs are strongly bound (~0.3 eV), excitonic effects are important even at room temperature. One clue to the origin of the linewidths is the correlation between nanotube diameter

and emission linewidth:[26] the linewidth is broader in smaller diameter nanotube at room temperature. A possibility is that this broadening originates from the dephasing time of excitons in the ground state due to exciton-phonon scattering, i.e. if the dephasing time is shorter for smaller diameter SWNTs. The role of exciton-phonon scattering is also apparent in temperature dependence of the linewidth, as described later in this chapter.

The absorption linewidth and shape is largely determined by carrier relaxation. In contrast with emission, PLE profile even from an individual nanotube can show several resonances. However, the E_{22} resonance is strongly dominant, with a Lorentzian lineshape of FWHM measuring about 40 meV. This linewidth is consistent with lifetime broadening at the timescales (<1 ps) measured in photobleaching experiments (See **chapter XX** on fast optics). For E_{22}, no significant systematic trend in linewidths as a function of (n,m) has yet been found.

3.2. Polarization. The optical response of SWNTs is strongly affected by its shape anisotropy, with both absorption and emission of photons having a strong polarization dependence. Anisotropic scattering was first demonstrated in Raman spectroscopy on individual nanotubes.[27] For surfactant SWNTs, this result was reproduced soon after the discovery of PL.[25] Fig. 7 shows the polarization dependence of both light absorption and PL emission. Both emission at E_{11} and absorption at E_{22} have a maximum intensity for polarization parallel to the nanotube axis. The intensity fits a $\cos^2\theta$ polarization dependence, and the polarization anisotropy was found to be ~20 in emission, and ~10 in absorption. Considering the enormous aspect ratio of these SWNTs, the measured anisotropy is actually quite small. However, those nanotubes deviated at least slightly from perfect straightness and any bend necessarily reduces the polarization anisotropy. Results of absorption anisotropy are now available on ensembles using post-growth alignment schemes or vertically grown nanotube forests.[28,29]

As discussed in section 2, perpendicular excitations are expected to be strongly suppressed due to the antenna effect.[2] Still, PLE spectra reveal distinct absorption peaks for different polarization configurations. Anisotropy in the PL for micelle-suspended SWNTs was first reported and it was shown that the degree of anisotropy was different for different fixed excitation wavelengths.[30] Polarized photoluminescence excitation (PLE) spectroscopy (i.e. with tunable excitation wavelength) on ensembles of smaller diameter nanotubes clearly showed cross-polarized absorption peaks.[31] In the cross-polarized configuration, excitation is transversely polarized with respect to emission. Using data obtained from the different configuration of polarization allows for 'pure' components of parallel (longitudinal) and perpendicularly (transverse) excitations to be extracted. Figure 8a shows a PLE map in the usual longitudinal configuration, while Figure 8b shows the transverse PL excitation map revealing resonances (horizontal arrows) attributed to E_{12} and E_{21} transitions. Those resonances appear close but at a different energy from the dominant E_{22} resonances. Within a non-interacting model, transition energies for the cross-polarized condition are expected halfway between E_{11} and E_{22}. However, the resonances observed in Fig. 8 appear close to E_{22}, thus at considerably higher energy than predictions within a single particle theory. This result provides further evidence for excitons in SWNTs. A blue-shift of excitonic E_{12} and E_{21} transitions relative to E_{11} is expected theoretically by correlated-electron calculations.[32] The amount of blue shift depends on the strength of Coulomb interaction. Similarly, a large blue-shift of an excitonic absorption peak for perpendicular polarization is expected on the basis of calculations that take into account the depolarization effect (See Chapter 7).[33] New polarized PLE imaging results clearly resolve E_{12} and other features, including their (n,m) dependence, and can be explained in the context of these excitonic pictures.[34]

3.3 **Quantum efficiency**. The quantum efficiency (η) is a parameter of great interest from the point of view of basic physics as well as from the point of view of photonic and optoelectronic applications. It can be defined as the ratio of the number of photons emitted (n_{em}) to the number of photons absorbed (n_{abs}), so that $\eta=n_{em}/n_{abs}$. For SWNTs in a surfactant, early reports suggested $\eta\approx0.1\%$, but much higher values have been measured recently. These numbers represent only estimates since either or both photon numbers (n_{em} and n_{abs}) have not been measured directly.

For nanotubes in solution, the number of absorbed photons at a given energy is straightforward and is measured simply by looking at the optical density of the solution. Solutions with optical density of order OD=0.1 are often used (corresponding to transmission of 80%). Non-SWNT absorbers must be negligible or accounted for in some way. Ideally, all absorbed photons excite SWNTs in the solution. If the nanotubes were pristine and perfect, PL would not be expected from the metallic fraction (so $\eta=0$), and would be a maximum for semiconductors ($\eta=\eta_{max}$). For bundles, or individual SWNTs that are defective,

short with end effects, kinked or otherwise imperfect, the efficiency will be lower ($\eta<\eta_{max}$). In ensemble measurements one is averaging over a distribution, and so can only determine a lower bound on the intrinsic η of pristine SWNTs. Of course, SWNT PL is possible over a large range of wavelengths, and the detector must be sensitive to all possible emitters in the sample. One must also be careful to take into account the collection efficiency of the optical system.

It is more straightforward to determine η for an individual SWNT of known diameter and length. In that case, in terms of experimentally accessible parameters, $\eta=P_e\lambda_e S/AP_i\lambda_i S_T$ where P_i , λ_i and S are respectively the incident laser power, wavelength and spot area, and A is the fraction of incident photons absorbed by the nanotube, P_e, is the power emitted from the tube, λ_e the emission peak wavelength, and S_T is the surface area of the SWNT. Like molecules, SWNTs are expected to be transparent to most incident photons, so that A<<1. Measurements of A are not available at the single nanotube level, however, ensemble measurements yield an optical cross-section of 1.6×10^{-4} nm^2 per carbon atom,[28] and with a surface density of carbon atoms in graphene of 37 carbon atoms/nm^2, the absorption coefficient of a SWNT is estimated at A=0.0059 (i.e. a SWNT absorbs one out of 169 incident photons). With PL imaging and spectroscopy, all parameters except A are determined and the SWNT quantum efficiency is estimated at η=7%, a value significantly higher than previous reports.[35]

A low η might be expected by comparison to similar materials. For example, in conjugated polymers a low η is understood to arise from optically dark states, which are lower in energy than the optically bright state. However, in SWNTs, these states are expected to be just below the bright exciton (about 1 meV below) and therefore only significant at low temperatures (of order 10K).[36] Loss of PL intensity has been seen in this temperature range,[37] and recent temperature and magnetic field dependent measurements strongly support this picture.[38]

Three factors may cause η to be (n,m) dependent: E_{22} absorption rates, E_{11} emission rates, and relaxation process between the two states. These may have intrinsic as well as extrinsic components. Intrinsic aspects have begun to be investigated theoretically.[39,40] Within a non-excitonic model, optical absorption at E_{22} is found to depend strongly on chiral angle while the diameter dependence is weak. For emission at E_{11} the dominant dependence is in diameter. On this basis, PL intensities would be greater for smaller diameter nanotubes of the mod2 family, with emission from near zigzag angle SWNTs being most intense. In contrast, there is a virtual absence of signal from near zigzag SWNTs in PLE maps, however (n,m) distributions are not likely to be uniform. The phonon relaxation process from E_{22} to E_{11} results in lower η for mod2 and near zig-zag SWNTs. This is because, for the mod2 family with its smaller E_{22}/E_{11} ratio, interband splitting becomes less than the LO phonon energy, closing a relaxation pathway and so dramatically slowing relaxation to E_{11} (see also Chapter 8).

A relaxation picture involving a process where two E_{11} excitons are created was used to explain weak PL in near-zigzag SWNTs.[40] This extra decay channel should be possible in mod1 nanotubes for which $E_{22}>2E_{11}$, but not for mod2 nanotubes. Independent experimental evidence, for example larger absorption linewidths for shorter decay times, has not yet been obtained.

3.4 Photoluminescence Imaging. SWNTs are often grown to millimeter lengths or more. This means that despite their nanometer scale diameters, they are macroscopic objects and they can produce an extended, resolvable optical image in the far field.

PL imaging of individual nanotubes in the far field has been reported for detection with near infrared 2D detectors and laser illumination,[15,35,41] as well as white light illumination.[42] A PL image of a single SWNT suspended over a trench is shown in Fig. 9a, with the corresponding PL spectrum shown in Fig. 9b. Spatially resolved spectroscopy shows that for individual nanotubes in surfactant gels, PL linewidths are usually ~30 meV, but occasionally only ~12 meV, in line with air suspended nanotubes.[15] On extended images, small spectral shifts (~2 meV) have been reported from end-to-end of a single such nanotube. Such shifts and broadening have been interpreted in terms of the different environmental effects along the length of the nanotube. On freely suspended SWNTs,[35] while most nanotubes had fixed emission wavelengths, small shifts in emission were seen in some nanotubes, possibly attributable to changes in the local environment along the lengths of the single nanotubes. Large spectral shifts were also seen and attributed to (n,m) changes.

PL imaging with deep sub-micron resolution is also possible using scanning probe near field techniques (see **Chapter XX** on new techniques).[43] For SDS wrapped SWNTs on mica, "hotspots", ~20 meV shifts and significant linewidth variations have been observed with ~15 nm resolution on micron

length nanotubes.[44] These are presumably all environmental effects related to the micelle wrapping. Such methods have also been used to detect and spatially resolve nanotubes directly on glass.

3.5 Time Dependence. Ultrafast optical studies (from ps to μs timescales) give detailed information about the dynamics of the PL process and are covered in detail in **Chapter XX.** Here we discuss only very slow (ms to ks timescale) fluctutations in PL intensity which are sometimes observed. The experimental results are quite diverse and depend on experimental conditions. For SWNTs suspended above a substrate, stable PL is obtained, and this is sometimes the case in solution. Time-dependent PL can be caused by high excitation intensities, temperature fluctuations, fluctuations in ambient environment, pH changes, gas ambient changes and other effects. For surfactant coated SWNTs deposited on substrates, random fluctuations of PL intensity (blinking) and/or PL wavelength (spectral diffusion) have been seen, especially at low temperatures (See Fig. 10). Presumably, these random fluctuations are the consequence of local defects on the nanotube or in its immediate surrounding, and these defects change the nanotube environment dynamically by trapping and releasing charged or neutral excitations. Blinking was observed even at room temperature in similar samples, and explained the same way.[45]

In contrast, the vast majority of air suspended SWNTs show steady luminescence at low excitation power. However, some do show slow intensity variations and gradual dimming.[35] This phenomena is associated with the "pushing down" of suspended SWNTs by optically induced forces and was first seen by global Raman imaging.[46] In that case, SEM observation of the nanotubes showing losses of Raman intensities confirmed that they collapsed down onto the substrate.

3.6 Phonons. Optical processes described so far in this chapter involved solely electron-hole excitations. This is reasonable for a first description since they represent the by far the strongest resonances in the PLE map. There are however a number of additional weaker features, some of them which can be assigned to phonon-assisted processes. These appear as satellites of the main E_{11} and E_{22} resonances. In one spectacular example, several phonon sidebands including overtones are observed in low temperature PLE on individual SWNTs.[47] Fig. 11 shows an example of an E_{11} phonon sideband.[48] The excitation energies have been offset by the corresponding E_{11} emission energy to highlight the common phonon feature. There is a clear peak around 200 meV above E_{11} which corresponds to the energy of the *G*-band phonon. This is described as an exciton-phonon complex and theory predicts that the strength of this sideband is much greater within an excitonic picture, and it would not be visible in a non-excitonic picture.[49]

Phonon sidebands are not limited to E_{11} excitons, but also originate in other exciton bands such as E_{22}. An experimental demonstration of the relation of an E_{22} sideband to phonons was provided by comparing PL of SWNTs made from different carbon isotopes.[50] A slight spectral shift occurs when ^{13}C is used instead of ^{12}C. The spectral weight of this sideband is of order of a few percent, in agreement with theory.[49]

4. Physical and chemical effects.

4.1 External environment. All atoms in SWNTs are surface atoms, and furthermore SWNTs are miniscule, so SWNT physical and chemical properties, including PL, depend greatly on the immediate surroundings. Effects of the environment are seen whether the luminescent nanotubes are in a surfactant solution - whether neutral or ionic - or a solid matrix, suspended in air or other ambient gas or in direct contact with a substrate or even contacting other nanotubes.

One way the environment can affect the nanotube properties is by changing its electrostatic surrounding. This may occur simply by dielectric screening, or through the transfer of electric charge. The effect of dielectric screening on the PLE map was discussed in section 2.3, and the theory is discussed in detail in Ch. 6. Briefly, the electron-hole dipole produced by photon absorption will displace surrounding charges, effectively reducing the Coulomb interaction between the electron and hole. Theory predicts that increased dielectric screening (i.e. weaker interaction) leads to a redshift of E_{11} and E_{22} transitions, because the self energy correction (redshift with increasing screening) is generally greater than the exciton binding energy (blueshift with increasing screening). Simple scaling relationships have been found for the exciton binding energy as a function of dielectric constant. Fig. 5 shows the difference (of order 10 meV) in E_{11} and E_{22} energies for air ambient as compared to surfactant solutions. Sensitivity to ambient is also shown in Fig. 12 where shifts in E_{11} are attributed to molecular adsorption and desorption on the SWNT.[51]

In environments where charge transfer occurs to the SWNT, effects on the PL are more severe. For SWNTs in an ionic solution, changing the pH affects the charge state of the nanotube, leading to the suppression of both light emission and absorption.[52] This can be understood because the addition of charges shifts the Fermi energy from the mid-gap region toward and ultimately into the conduction or valence band. Light absorption in SWNTs is strongly resonant, and electrostatic doping removes or adds electron from those resonant states and light absorption is necessarily suppressed. In contrast with light absorption, which is usually only sensitive to state filling, light emission can also be very sensitive to the presence of dopants as reactive centers. Indeed, *p*H-dependent PL studies show that the PL intensity diminishes while absorption is largely unchanged (Fig. 13). Within their radiative lifetime (estimated at ns) E_{11} excitons can diffuse towards these reactive centers, where PL is quenched by non-radiative decay. A small number of charges can also quench PL through non-radiative Auger recombination.[52] These two processes are faster (taking only ~10 ps) than radiative decay rates and therefore dramatically lower PL intensities. The charge state can also be changed through capacitive gating, described in section 4.2.

The surrounding matrix, especially solids, can induce strain on an SWNT and so alter PL emission. An isotropic strain produces predominantly a radial stress on a long nanotube which can be viewed primarily as uniaxial stress on the graphene sheet. Within a TB model, the anisotropic distortion of the graphene sheet results solely in a shift of the Fermi points. For a metallic nanotube, this leads to the opening of a gap, while for semiconducting nanotubes to an increase of E_{11} and a reduction of E_{22} energies for the *mod1* family, and to an opposite shift for *mod2* with a diameter independent $\cos 3\theta$ functional form (see Chapter 6).[53] This effect was observed in PL for SWNTs frozen in an ice matrix where the strain results in large shifts.[54] The large axial strain produced by mismatch of the thermal expansion coefficients was estimated at 0.5% corresponding to a stress of 5 GPa. In contrast, PL experiments in liquid with hydrostatic pressures up to 1 GPa were found to decrease E_{11} and E_{22} energies, irrespective of the family.[55] This was attributed to a higher-order effect beyond the graphene-electron model. Recently, uniaxial strains have been applied, stretching individual SWNTs resulting in small shifts in PL peak position.[56]

4.2 External physical parameters. The previous section showed that temperature can be used indirectly to affect the strain on the nanotube in a matrix. In such samples, intrinsic temperature effects are mixed with strain effects and the two contributions must be disentangled. For freely suspended SWNTs, matrix effects are minimized, and experiments have been carried out down to the single nanotube level, with PL spectra obtained from 4K to 700K.[37,51] At low temperatures, the ambient must be controlled since the condensation of atmospheric gases causes a quenching of SWNT PL. Fig. 14 shows single SWNT data with changes in emission energy and linewidth as well as the emergence of additional peaks near 5K. Not shown here, intensity changes, shifts in absorption peak position, and the emergence of many unseen peaks also occur at low temperature.

The E_{11} PL emission peaks blueshift from 300K down to low temperature, with a species dependent magnitude ranging from almost zero to ~-50μeV/K. This is an order of magnitude less than conventional bulk semiconductors, and is important in applications such as lasers, where heating can shift the bandgap and consequently reduce gain and efficiency. This data is well fit theoretically by a TB model which includes only electron-phonon interaction, not excitonic effects.[57] The model predicts a family pattern for the shift, and for some species of the *mod2* family, the bandgap shows a more complex dependence, with a redshift at temperatures below 100K. The temperature dependence of all E_{11} species is predicted by a "Vina"-type equation which including two phonon-related effects (see Chapter 6). A more complete experimental study measuring the temperature dependence of the PL for many (*n*,*m*) has not yet been reported.

Interestingly, at high temperatures a sudden shift in PL peak position has been found to occur (a "bandgap shift transition").[51,58] This abrupt blueshift (~30 meV) on heating, which can take place over a few degrees, is larger than that the entire redshift which occurs between 5K and room temperature. As described in section 4.2, this effect is not thought to be intrinsic, but rather interpreted as a result of the outgassing of atmospheric adsorbates from the SWNT surface.

The linewidth and the intensity of the PL peak can provide insight into the PL mechanism. In several reports on individual SWNTs and SWNT ensembles, the linewidth narrows linearly from 300K to 4K, while the integrated intensity increases modestly as temperature is reduced from 300K to leveling off and ultimately decreasing from about 50K to 4K. The temperature dependence of the linewidth in Fig. 14 shows a linear drop from 9 meV to 2 meV between 300 and 4K. Sub-meV linewidths have also been reported at low temperature for nanotubes in contact with a substrate.[59] It should be noted that in such

samples blinking and spectral diffusion was also observed, suggesting that extrinsic factors are important, such as substrate induced or on-tube defects. It is worth noting that Raman features often have narrow linewidths overlapping the SWNT PL emission range, and care must be taken in assigning spectral features to radiative recombination.

Time-resolved PL decay experiments are essential complements to CW PL data, especially to help explain the trends observed in emission intensity and linewidth. Detailed discussion of time resolved data can be found in **Chapter XX** on fast optics). Briefly, for single SWNTs, a mono-exponential decay is observed with timescales from order 10 ps to 100 ps. Variability of timescale is a sign of sample inhomogeneity.[60] In SWNT ensembles, this tube-to-tube variation in decay rates leads to multiple exponential decay curves. A detailed temperature study of the long timescale component (~100 ps) shows a fivefold increase of the decay time from 300K and saturation and decrease below 50K.[36] This result correlates exactly with the emission intensity, and is also consistent with the temperature dependence of the linewidth. The mechanisms responsible for the high and low temperature behavior are competing radiative and non-radiative channels of the bright and dark exciton states. Above 50K, excitons in the lowest energy dark states are thermally excited to the bright exciton state; therefore, the most significant and relevant decay channel at elevated temperatures is through the bright exciton state. For the bright state alone, both radiative and non-radiative processes compete, with the latter being phonon mediated. At low temperature, the dark exciton state becomes an effective non-radiative channel for exciton decay, as excitons trapped in those states can no longer be thermally excited to the bright state. These experiments allow for an estimate of ~4 meV for the dark-bright exciton splitting (see Chapter 13).

Since the dark exciton-bright exciton energy splitting is small, weak symmetry breaking perturbations can significantly change SWNT PL, either by altering the band ordering, or by changing state mixing. Brightening of PL intensities is observed when high magnetic fields (>1 T) are applied along the SWNT axis, providing the most direct evidence of low energy dark excitons in SWNTs.[38,61,62] This effect and its physical origin is described in detail in Chapter 13. The existence of dark excitons has been proposed to reduce SWNT PL quantum efficiencies, however because of the small splitting this effect appears minimal at room temperature.[38]

An electric field also affects PL, by breaking the symmetry or by changing the SWNT charge state. A suspended SWNT can be electrically connected in a nanotube field effect transistor (FET) configuration (see Chapters 14 and 15). In such a device, the capacitive coupling to the conductive substrate allows for charge to be drawn in and out of the nanotube, and in addition to measuring electrical conductivity, PL spectra can be acquired. Fig. 15 shows that the PL intensity peaks at negative gate voltages, while the spectral shape remains qualitatively unchanged.[63] The peak corresponds to the onset of hole conduction. It was also found that electric current suppresses PL intensity. The analysis is based on a free-electron and free-hole picture, and must be revised in the light of the excitonic picture. In analogy with pH dependent studies, we might expect that excess charge in electrostatically doped nanotubes should also lead to a suppression of the luminescence, most likely through the creation of new Auger process decay channels.

5. Applications

5.1 **Nanotube research**. The advance of research in any materials system is intimately linked to the ability to evaluate the outcome of synthesis and fabrication. While other methods, either direct like TEM, or indirect, like resonant Raman spectroscopy can provide structural information, the PLE mapping method has emerged as arguably the most effective way to determine (n,m) distributions for semiconducting SWNTs. Other methods can provide similar data, and even be more direct, but PLE mapping is rapid, relatively economical, and reliable, and can be used at the ensemble or even down to the single nanotube level. PLE mapping systems are already available commercially.

The weaknesses of PLE mapping are discussed in detail in Chapter 3. Briefly, first, metallic nanotubes are not seen in PLE maps. Estimating the relative abundance of a given ($\underline{n}$,m) species within a sample is a delicate undertaking if one does not simply count nanotubes. There is not yet a generally accepted calibration as to the relative brightness of different species. Selection effects are possible, especially in solution, as there may be extrinsic environmental effects which preferentially weaken the luminescence of certain species. If SWNTs are not well isolated, it is already clear that energy transfer between nearby isolated nanotubes or within bundles can occur,[16] and this must be species dependent. Defects should reduce luminescence efficiency with their abundance or effect being likely (n,m) dependent.

Despite its weaknesses, PLE mapping remains a very effective method of estimating (*n*,*m*) distributions, especially when comparing relative abundances of like samples.

5.2 **Wider applications**. SWNTs are prime candidates for sensing applications, because interactions with the surface are a basis for sensing and for SWNTs, every carbon atom is on the surface and can potentially contribute. As described in section 4, light emission in SWNTs is affected in several ways when the local environment changes. Potentially, the sensitivity of SWNT PL to the local environment could be used for sensing in a broad range of applications. At the present, the challenge is to carefully characterize SWNT PL sensing, and determine whether or not this kind of sensing is competitive with existing technologies.

One can foresee that SWNT sensors based on light detection could have several advantages including ease of implementation (relative to electronic based sensing), flexibility in the choice of embedding matrix (either free in solution or fixed on a substrate), the potential for ultra-high packing density, and chemical specificity (through attachment of various functional groups). That SWNTs emit in the near-infrared may appear to be a drawback. However, detector sensitivity in the near-IR has improved significantly in recent years, and sensitive cameras are becoming less and less expensive. In addition, IR emission is desirable in specific applications where an emission background is present in the visible range.

A specific sensing application is fluorescent dye labeling in biological systems. Biological activities from the organism-level to the molecular level activity can be monitored by imaging PL from dyes. Dyes must be bio-compatible with the subject, alive or not, and should show strong PL in a fixed band. Some dye molecules (or "fluorophores") are not benign and for example may be toxic to a cell under investigation. The main weakness of common fluorophores is their sensitivity to photobleaching, meaning they can degrade under photoexcitation. SWNTs are very promising as fluorophores and are actively being investigated in this context. There is no evidence of blinking or photobleaching in SWNTs after prolonged exposure to excitation at high intensity.[64] SWNTs also have a reasonably high quantum efficiency,[35] and many distinct species (and thus potentially many distinct fluorophores) emit in the portion of the near infrared band which is largely transparent in biomaterials. Absorption by liquid water limits the usefulness of larger diameter nanotubes for this application. It is quite possible that SWNTs, at least in small quantities may be benign in biological systems. For example, it has been demonstrated that cell division can occur in cells incorporating luminescent nanotubes.[65] However, much more research will be required to determine what effects SWNTs have on biological systems, good or bad, and what SWNT concentration would be required to cause such effects. It is presently unclear what health risks (or benefits) SWNTs might pose, if any.

Electronic applications of SWNTs are promising in large part because of their remarkable current carrying capacity. Since the discovery of PL in SWNTs, interest has grown in their optoelectronic properties. In electroluminescence (EL) light emission occurs with purely electrical excitation, as opposed to optical excitation in PL, as for example at the interface of a *p-n* junction, by impact excitation, and by the creation of hot carriers.[66,67] Likewise, light absorption by SWNTs can give rise to electrical signals, with photoconductivity,[68,69] and bolometry,[70] now being actively explored. Thus applications arise from PL alone, but also by characterizing SWNT luminescence and absorption, PL data motivates and assists in the development of nanotube based optoelectronic devices.

6. Conclusion

The field of SWNT PL is in a rapid growth phase. Basic features of SWNT PL have been uncovered, and explained in this chapter, but there is vastly more which is only beginning to be investigated. Preparing SWNTs such that they emit PL at all was an early challenge, but now surfactant-liquid, surfactant-solid and air-suspended preparations are well established and successful. PL from SWNTs has such remarkable attributes as (*n*,*m*) dependence, high quantum efficiency, strong polarization dependence, sub-*kT* linewidths and characteristic lineshapes. The method of PLE mapping has emerged as a popular method for (*n*,*m*) assignment, and features in the PLE map beyond E_{11} and E_{22} are being systematically explored. Not just spectroscopy, but also PL imaging is growing in importance. The effect of the dielectric environment, charge transfer, temperature, strain, electric field, magnetic field and similar effects have all been explored to some extent, but not in a comprehensive way. Over the past couple of years, the excitonic origin of SWNT PL has been explored extensively, with large bandgap renormalization and exciton binding effects seen and the role of dark excitons being uncovered. The SWNT is a model system for one-dimensional exciton physics. The exploration of systematic trends in PL as a function of

(*n*,*m*) is becoming even more important, and is especially interesting because changing (*n*,*m*) allows one to "tune" diameter and chirality.

As has been the case for more established material systems, it is likely that much of the future work on SWNT PL will relate to improvements in sample preparation. Until recently the SWNT has usually been viewed as an ideal, perfect lattice, in a perfectly featureless background. It is of course expected, and already there is considerable evidence that SWNT PL is sensitive to many of the real-world deviations from this idealized picture. We can expect a systematic understanding, experimental and theoretical of how deviations from ideality affect SWNT PL. For example, dopant densities, adsorbates, defects, end effects, chemical functionalization and surface effects remain to be systematically studied and the mechanisms underlying their effects remain to be fully elaborated. The collective effects on PL of combinations of SWNTs either in bundles, crossing, in junctions or as shells of DWNTs will be an important area of SWNT PL work in future years. We can expect better and better SWNT samples for PL, and in return PL will likely only grow in importance as a method of characterizing SWNT samples. Of course, there have already been surprises with almost every experiment and there is likely almost as much that is unpredictable in the road ahead.

It has largely been fundamental scientific interest that has been driving research into SWNT PL. However, SWNT PL studies have uncovered diverse phenomena which could be exploited technologically. New applications in biology, medicine, photonics and optoelectronics appear to hold promise as we look to the future, and we expect these applications to increasingly drive applied research in SWNT optics in the future.

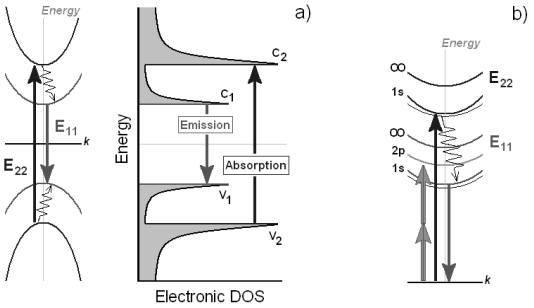

Figure 1. Optical processes in SWNTs. (a) The band structure and optical transitions in a simplified single particle picture and its corresponding density of states. Light absorption at E_{22} is shown with an upward-pointing arrow and light emission at E_{11} is shown with a downward-pointing arrow. The thin jagged arrows illustrate relaxation from E_{22} to E_{11}. (b) A simplified picture of the exciton band structure and optical transition. One photon processes are shown as in (a) and a two-photon process is shown with two gray upward-pointing arrows. The ground state represents a vacuum state, that is, with no excitons.

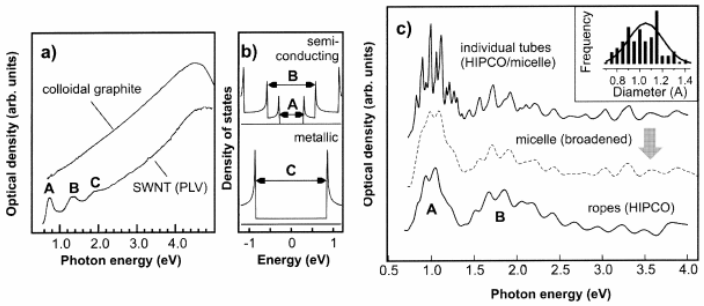

Figure 2. Optical absorption from SWNT ensembles using different preparation methods. (a) Raw spectrum from SWNTs and graphite. (b) Illustration of interband process giving rise to the absorption peaks. (c) Effect of sample preparation an absorption resonance for a background subtracted spectrum. The inset shows the diameter distribution. (From Ref. [6])

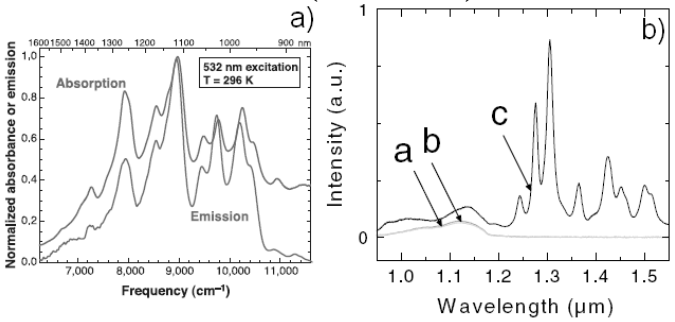

Figure 3. (a) Optical emission and absorption from an ensemble of isolated SWNTs in a surfactant solution. Taken from Ref. [1]. **(b)**. PL from a small number of SWNTs suspended freely above a substrate. Samples without suspended SWNTs do not show SWNT PL (labels a, b) while areas with suspended SWNTs show sharp PL peaks (label c). (From Ref. [9])

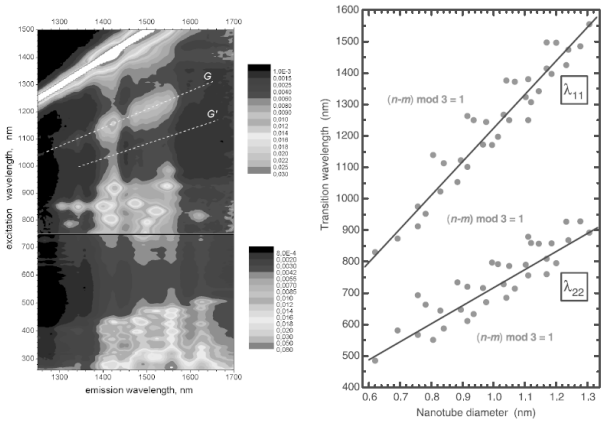

Figure 4. (a) A photoluminescence excitation map from an ensemble of SWNTs in a surfactant solution. (From Ref. [11]) (b) A Kataura plot derived from photoluminescence data from a SWNT solution. (From Ref. [12])

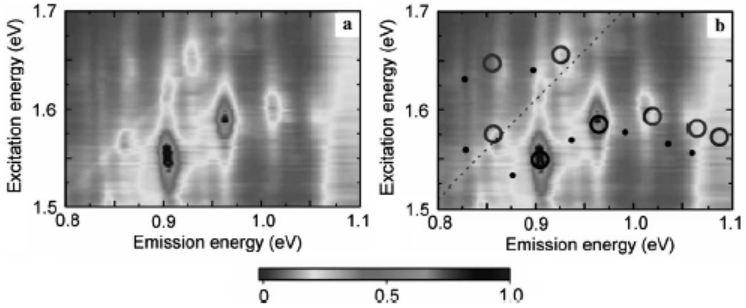

Figure 5. A photoluminescence excitation map from an ensemble of freely suspended SWNTs. (a) shows the data only. In (b) corresponding surfactant nanotubes peaks are labeled as black dots, and circles show the surfactant peaks plus a fixed energy offset which provides the best fit with the air suspended peak positions. (From Ref. [14])

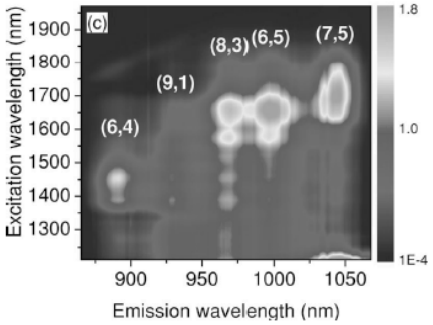

Figure 6. A photoluminescence excitation map obtained in a two-photon absorption experiment. (From Ref. [22])

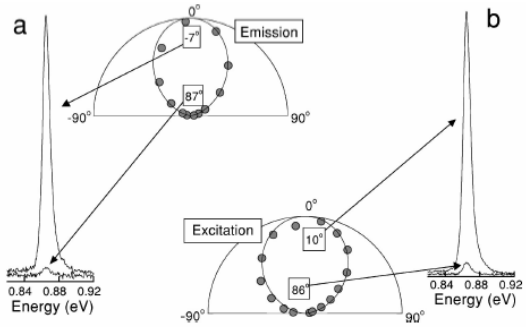

Figure 7. Polarization dependence of PL emission (a) and excitation (b). (From Ref. [10])

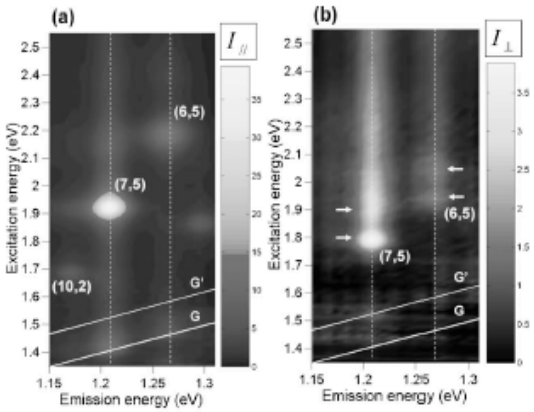

Figure 8. Longitudinal (a) and transverse PL excitation map. The resonances in (b) are attributed to absorption into E_{12}. Horizontal arrows indicate transverse resonances (From Ref. [31])

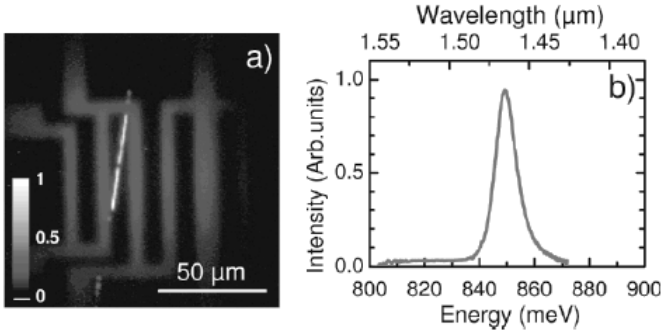

Figure 9. (a) A PL image of an individual SWNT freely suspended in air above a patterned Si substrate. (b) The PL spectrum of the nanotube in (a). (From Ref. [35])

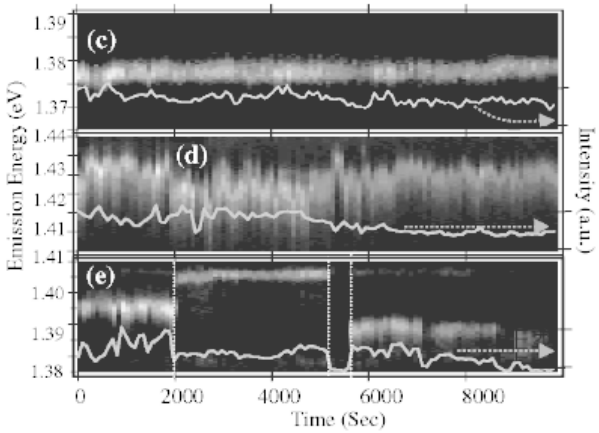

Figure 10. Time evolution of photoluminescence spectrum from individual SWNTs on a substrate measured at low temperature. In (c), the emission is constant and the intensity fluctuates, while in (d) and (e), both emission energy and intensity fluctuate. (From Ref. [59])

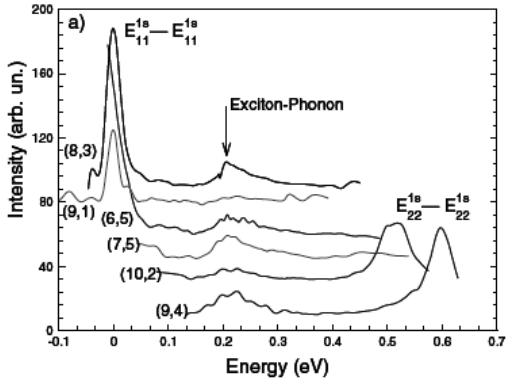

Figure 11. PL excitation profile just above E_{11} showing phonon-assisted absorption (peaks around 200 meV). The energies have been offset by the corresponding E_{11} energy. Peaks visible at higher energy correspond to E_{22} absorption. (From Ref. [48])

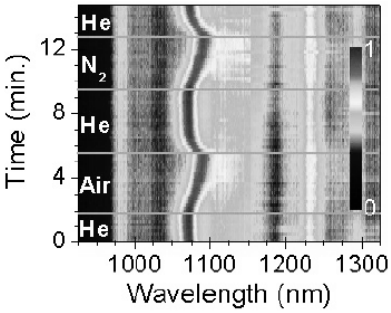

Figure 12. Dynamics of the photoluminescence peak position upon cycling of the gas ambient. (From Ref. [51].)

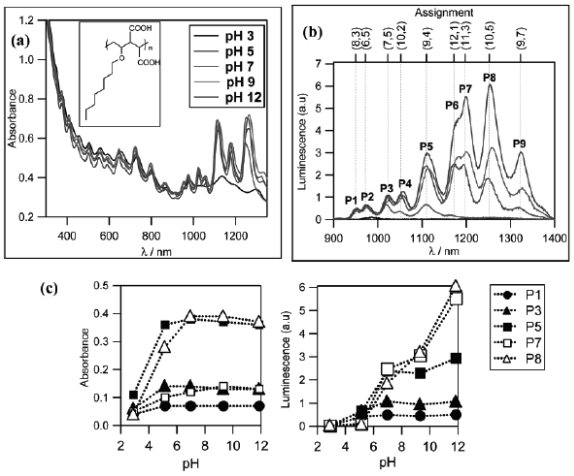

Figure 13. The pH-dependence study of absorbance (a and c) and luminescence (b and d) in SWNT ensembles. A decrease in pH leads to a suppression of both light absorption and emission. (From Ref. [52].)

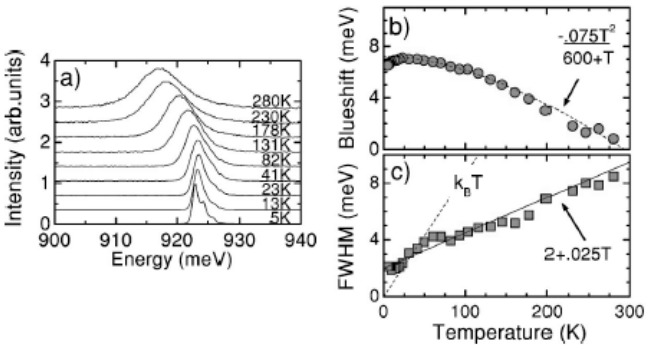

Figure 14. Temperature dependence of the luminescence from a single freely suspended SWNT (a) PL spectra from 280 to 5 K. Evolution of (b) peak position (c) linewidth. In (c), the thermal energy $k_B T$ is plotted for comparison. (From Ref. [37]).

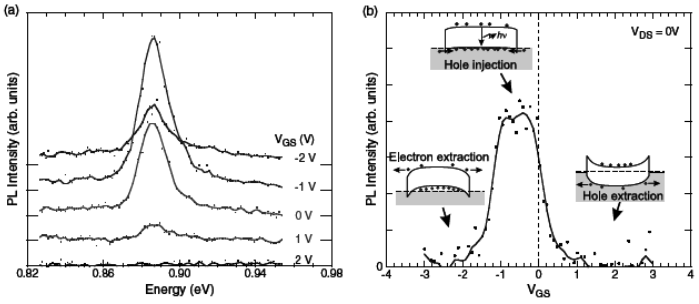

Figure 15. Electric field dependence of PL for a suspended SWNT in a nanotube field effect transistor. (a) PL spectra taken at various gate voltages. (b) PL intensity versus gate voltage showing a maximum at a flat band condition as illustrated in the inset. (From Ref. [63].)

---

[1] M. J. O'Connell, S. M. Bachilo, C. B. Huffman, V. C. Moore, M. S. Strano, E. H. Haroz, K. L. Rialon, P. J. Boul, W. H. Noon, C. Kittrell, J. Ma, R. H. Hauge, R. B. Weisman, and R. E. Smalley, Science **297,** 593 (2002).

[2] H. Ajiki, and T. Ando, Jpn. J. Appl. Phys. Suppl. **34-1**, 107 (1995).

[3] T. Ando, J. Phys. Soc. Jpn. **66**, 1066 (1997).

[4]H. Kataura, Y. Kumazawa, Y. Maniwa, I. Umezu, S. Suzuki, Y. Ohtsuka, , Y. Kumazawa, Y. Maniwa, I. Umezu, S. Suzuki, Y. Ohtsuka, Y. Achiba,. Synth. Met. 103, 2555 (1999).

[5] O. Jost, A. A. Gorbunov, W. Pompe, T. Pichler, R. Friedlein, M. Knupfer, M. Reibold, H.-D. Bauer, L. Dunsch, M. S. Golden, and J. Fink Appl. Phys. Lett. **75,** 2217 (1999).

[6] A. Hagen and T. Hertel, Nano Letters **3**, 383 (2003).

[7] J. Kong, A. M. assel, and H. Dai, Chem. Phys. Lett. **292**, 567 (1998).

[8] Y. Homma, Y. Kobayashi, T. Ogino, and T. Yamashita, Appl. Phys. Lett. **81**, 2261 (2002).

[9] J. Lefebvre, Y. Homma, and P. Finnie, Phys. Rev. Lett. **90**, 217401 (2003).

[10] J. Lefebvre, J. M. Fraser, P. Finnie, and Y. Homma, Phys. Rev. B **69**, 075403 (2004).

[11] S. Lebedkin, K. Arnold, F. Hennrich, R. Krupke, B. Renker, and M. M. Kappes, New J. of Phys. **5**, 140 (2003).

[12] S. M. Bachilo, M. S. Strano, C. Kittrell, R. H. Hauge, R. E. Smalley, and R. B. Weisman, Science 298, 2361 (2002).

[13] S. Bachilo, and R. B. Weisman, Nano Lett. 3, 1235 (2003).

[14] J. Lefebvre, J. M. Fraser, Y. Homma, and P. Finnie, Appl. Phys. A: Mat Sci. & Proc. **78**, 1107 (2004).

[15] D. Tsyboulski, S. M. Bachilo, R. B. Weisman *Nano Lett.,* **5** (5), 975(2005).

[16] O. N. Torrens, D. E. Milkie, M. Zheng, and J. M. Kikkawa, Nano Lett. **6**, 2864 (2006).

[17] T. Hertel, A. Hagen, V. Talalaev, K. Arnold, F. Hennrich, M. Kappes, S. Rosenthal, J. McBride, H. Ulbricht, E. Flahaut, Nano Letters **5**, 511 (2005).

[18] T. Okazaki, S. Bandow, G. Tamura, Y. Fujita, K. Iakoubovskii, S. Kazaoui, N. Minami, T. Saito, K. Suenaga, S. Iijima, Phys. Rev. B **74**, 153404 (2006)

[19] C. L. Kane, E. J. Mele, Phys. Rev. Lett. **90**, 107401 (2003).
[20] E. J. Mele and C. L. Kane, Sol. Stat. Comm. **135**, 527 (2005).
[21] F. Wang, G. Dukovic, L. E. Brus, and T. F. Heinz, Science **308**, 838 (2005).
[22] J. Maultzsch, R. Pomraenke, S. Reich, E. Chang, D. Prezzi, A. Ruini, E. Molinari, M. S. Strano, C. Thomsen, and C. Lienau, Phys. Rev. B 72, 241402 (2005).
[23] K. Hata, D. N. Futaba, K. Mizuno, T. Namai, M. Yumura, S. Iijima, Science **306**, 1362 (2004).
[24] D. A. Tsyboulski, S. M. Bachilo, and R. B. Weisman, Nano Letters **5**, 975 (2005).
[25] A. Hartschuh, H. N. Pedrosa, L. Novotny, and T. D. Krauss, Science 301, 1354 (2003).
[26] T. Inoue, K. Matsuda, Y. Murakami, S. Maruyama, and Y. Kanemitsu, Phys. Rev. B **73**, 233401 (2006).
[27] Duesberg et al., Phys. Rev. Lett. **85**, 5436 (2000).
[28] M. F. Islam, D. E. Milkie, C. L. Kane, A. G. Yodh, J. M. Kikkawa, Phys. Rev. Lett. **93**, 037404 (2004).
[29] Murakami et al., Phys. Rev. Lett. **94**, 087402 (2005).
[30] Lebedkin et al., J. Phys. Chem. B **107**, 1949 (2003).
[31] Miyauchi et al., Phys. Rev. B 74, 205440 (2006).
[32] Zhao and Mazumdar, Phys. Rev. Lett. **93**, 157402 (2004).
[33] Uryu and Ando, Phys. Rev. B **74**, 155411 (2006)
[34] J. Lefebvre, P. Finnie, Phys. Rev. Lett. **98**, 167406 (2007).
[35] J. Lefebvre, D. G. Austing, J. Bond, P. Finnie, Nano Lett., **6** (8), 1603-1608 (2006).
[36] S. Berger, C. Voisin, G. Cassabois, C. Delalande, P. Roussignol, X. Marie, Nano Lett. **7**, 398 (2007).
[37] J. Lefebvre, P. Finnie, and Y. Homma, Phys. Rev. B **70**, 045419 (2004).
[38] I. B. Mortimer, R. J. Nicholas, Phys. Rev. Lett. **98**, 027404 (2007).
[39] Y. Oyama, R. Saito, K. Sato, J. Jiang, Ge. G. Samsonidze, A. Grüneis, Y. Miyauchi, S. Maruyama, A. Jorio, G. Dresselhaus, and M. S. Dresselhaus, Carbon **44**, 873 (2006).
[40] S. Reich, C. Thomsen, J. Robertson, Phys. Rev. Lett. **95**, 077402 (2005).
[41] P. Cherukuri, S. M. Bachilo, S. H. Litovsky, R. B. Weisman, J. Am. Chem. Soc. **126,** 15638 (2004).
[42] D. G. Austing, J. Lefebvre, J. Bond, P. Finnie, Appl. Phys. Lett., **90** 103112 (2007).
[43] A. Hartschuh, H. Qian, A. J. Meixner, N. Anderson, L. Novotny, J. of Lumin. **119-120,** 204 (2006).
[44] H. Qian, T. Gokus, N. Anderson, L. Novotny, A. J. Meixner, A. Hartschuh, Phys. Stat. Sol. (b) **243**, 3146 (2006).
[45] K. Matsuda, Y, Kanemitsu, K, Irie, T. Saiki, T. Someya, Y. Miyauchi, and S. Maruyama, Appl. Phys. Lett. **86**, 123116 (2005).
[46] K. Kaminska J. Lefebvre, D. G. Austing, P. Finnie, Phys. Rev. B **73** 235410 (2006)
[47] H. Htoon, M. J. O'Connell, S. K. Doorn, V. I. Klimov, Phys. Rev. Lett. **94**, 127403 (2005).
[48] F. Plentz, H. B. Ribeiro, A. Jorio, M. S. Strano, and M. A. Pimenta, Phys. Rev. Lett. **95**, 247401 (2005).
[49] V. Perebeinos, J. Tersoff, and Ph. Avouris, Phys. Rev. Lett. **94**, 027402 (2005).
[50] Y. Miyauchi, and S. Maruyama, Phys. Rev. B **74**, 035415 (2006).
[51] P. Finnie, Y. Homma, and J. Lefebvre, Phys. Rev. Lett. **94**, 247401 (2005).
[52] G. Dukovic, B. E. White, Z. Zhou, F. Wang, S. Jockusch, M. L. Steigerwald, T. F. Heinz, R. A. Friesner, N. J. Turro, and L. E. Brus, J., J. Am. Chem. Soc. **126**, 15269 (2004).
[53] L. Yang and J. Han, Phys. Rev. Lett. **85**, 000154 (2000).
[54] K. Arnold, S. Lebedkin, O. Kiowski, F. Hennrich, and M. M. Kappes, Nano Letters **4**, 2349 (2004).
[55] J. Wu, W. Walukiewicz, W. Shan, E. Bourret-Courchesne, J. W. Ager, K. M. Yu, E. E. Haller, K. Kissell, S. M. Bachilo, R. B. Weisman, and R. E. Smalley, Phys. Rev. Lett. **93**, 017404 (2004).
[56] H. Maki, T. Sato, and K. Ishibashi, Nano Lett. **7**, 890 (2007).
[57] R. B. Capaz, C. D. Spataru, P. Tangney, M. L. Cohen, and S. G. Louie, Phys. Rev. Lett. **94**, 036801 (2005).
[58] D. E. Milkie, C. Staii, S. Paulson, S., E. Hindman, A. T. Johnson, J. M. Kikkawa, Nano Lett. **5**, 1135 (2005).
[59] H. Htoon, M. J. O'Connell, P. J. Cox, S. K. Doorn, V. I. Klimov, Phys. Rev. Lett. **93**, 027401 (2004).
[60] A. Hagen, M. Steiner, M. B. Raschke, C. Lienau, T. Hertel, H. Qian, A. J. Meixner, and A. Hartschuh, Phys. Rev. Lett. **95**, 197401 (2005).
[61] L. J. Li, and R. J. Nicholas, Int. J. Modern. Phys. B **18**, 3509 (2004).
[62] J. Shaver, J. Kono, O. Portugall, V. Krstić, G. L. J. A. Rikken, Y. Miyauchi, S. Maruyama, V. Perebeinos, Phys. Stat. Sol (b) **243**, 3192 (2006).

[63] Y. Ohno, S. Kishimoto and T. Mizutani, Nanotechnology **17**, 549 (2006).
[64] D. A. Heller, S. Baik, T. E. Eurell, and M. S. Strano, Adv. Mat. **17**, 2793 (2005).
[65] P. Cherukuri, S. M. Bachilo, S. H. Litovsky, and R. B. Weisman, J. Am. Chem. Soc. **126**, 15368 (2004).
[66] J. A. Misewich, R. Martel, Ph. Avouris, J. C. Tsang, S. Heinze, and J. Tersoff, Science **300**, 783 (2003).
[67] J. Chen, V. Perebeinos, M. Freitag, J. Tsang, Q. Fu, J. Liu, and Ph. Avouris, Science **310**, 1171 (2005).
[68] M. Freitag, Y. Martin, J. A. Misewich, R. Martel, and Ph. Avouris, Nano Lett. **3**, 1067 (2003).
[69] I. A. Levitsky, and W. B. Euler, Appl. Phys. Lett. **83**, 1857 (2003).
[70] M. E. Itkis, F. Borondics, A. Yu, and R. C. Haddon, Science **312**, 413 (2006).